Performance Evaluation of a Trapezoidal Microchannel Heat Sink with Various Entry/Exit Configurations Utilizing Variable Properties

H. Khorasanizadeh[†] and M. Sepehrnia

Faculty of Mechanical Engineering and the Energy Research Institute, University of Kashan, Kashan, Iran

†*Corresponding Author Email: khorasan@kashanu.ac.ir*

ABSTRACT

Most of numerical studies on microchannel heat sinks (MCHS) performed up to now are for a two-dimensional domain using constant properties of the coolant and solid part. In this study, laminar fluid flow and heat transfer of variable properties water in a trapezoidal MCHS, consisted of five trapezoidal microchannels, are studied. The three dimensional solution domains include both the flow field and the complete MCHS silicon made solid parts with variable conductivity. Four entry/exit configurations and three pressure drops of 5, 10 and 15 kPa are assumed. The results indicate that the A-type heat sink, for which the entry and exit are placed horizontally at the center of the north and the south walls, has a better heat transfer performance, smaller thermal resistance and provides more uniform solid temperature distribution. For pressure drop of 15 kPa, temperature-dependent properties of water increases the heat transfer between 2.73% and 3.33%, decreases the thermal resistance between 3.46% and 5.55 % and decreases the ratio of difference between the maximum and minimum substrate temperatures to the heat flux, θ, between 3.42% and 11.15%. Also by assuming temperature-dependent conductivity of silicon, the heat transfer increases between 0.75% and 2.58%, the thermal resistance decreases between 1.15% and 4.97 % and θ decreases between 2.41% and 6.49%.

NOMENCLATURE

A	area	X, Y, Z	coordinates
c_p	specific heat		
D_h	hydraulic diameter	ρ	density
D	diameter	μ	viscosity
$\overline{h}$	overall heat transfer coefficient of heat sink	θ	the maximum temperature difference on substrate surface per heat flux
k	thermal conductivity		
L	length		
$\dot{m}$	mass flow rate	**Subscript**	
$\overline{\text{Nu}}$	average Nusselt number	avg	average
P	pressure	b	base plate
p	wet perimeter	ch	channel
Q_{flow}	heat absorbed by fluid	f	fluid
q	heat flux at microchannel heat sink base plate	fin	fin
		hs	heat sink
R_{th}	heat sink thermal resistance	in	inlet
Re	Reynolds number	max	maximum
T	temperature	min	minimum
V	fluid velocity	out	outlet
W	width	s	solid
		w	wal

1. INTRODUCTION

In very large scale integrated (VLSI) circuits, generation of high heat fluxes dictates a proper thermal management strategy. Otherwise amplified base plate temperature may lead to collapse of any electronic device. The concept of MCHS was firstly proposed by Tuckerman and Pease (1981). They investigated a heat sink with microchannels utilizing water as the coolant. Nowadays, microchannels, as closed circuits channels for fluid flow and heat removal are an essential part of the silicon-based electronic microsystems. Microchannels, with variety of cross sections and hydraulic diameters, provide many benefits such as higher heat transfer area, high heat transfer rates and lower coolant requirement (Tuckerman and Pease 1981), when compared with the conventional and millimeter sized channels.

Chein and Chen (2009) used water as the working fluid and studied entry/exit configuration effects on heat sink performance, numerically. They used 6 different configurations named I-, N-, D-, S-, U- and V-types. In the I-, N-, D- and S-types, the flow entered and left the heat sink horizontally, while in the U- and V-type the flow entered and left the heat sink vertically. They showed for the heat sinks with horizontal flow entry and exit, the velocity misdistribution through different microchannels was more serious than those of vertically flow supply and collection. To evaluate the performance, they studied the overall heat transfer coefficient, thermal resistance and pressure drop coefficient and found that the heat sink with vertically flow entry and exit performed better.

Ibáñez and Cuevas (2010) analyzed the entropy generation of magneto hydrodynamic flow that happens in a parallel plate microchannel, analytically. They observed that it is possible to minimize the total entropy generation rate with change of physical properties of the microchannel walls and fluid. Also it is dependent on the individual geometry or the operational condition of the microchannel.

Guo et al. (2011) investigated viscous dissipation effect on entropy generation of ethylene glycol and aniline in curved square microchannels, numerically. Their results showed that the frictional entropy generation and heat transfer entropy generation augment relatively due to viscous dissipation when the fluid was heated and a reverse trend was observed when the fluid was cooled. In a different numerical investigation, Guo et al. (2012) studied the effect of temperature-dependent viscosity of aniline and ethylene glycol on the thermodynamic performance of the same microchannel in laminar . When aniline was heated the frictional entropy generation number, the heat transfer entropy generation number and the Nusselt number were less when the viscosity was dependent on temerature compared with those of constant viscosity cases. However, the opposite trend noticed when aniline was cooled.

Hung and Yan (2012) studied the effect of tapered-channel design on microchannel heat sink performance, numerically. They found that the relationship between the thermal resistance and the width-tapered ratio at a fixed pumping power is not always agreeing. With width-tapered ratio increase the thermal resistance first decreased and then increased. A similar trend was also noticed when the height-tapered ratio increased. Also the width-tapered channel provided a more uniform temperature distribution along channel centerline compared to those of others.

Ibáñez et al. (2013) investigated the effects of slip flow on entropy generation and heat transfer for the two dimensional conjugate heat transfer in parallel wall microchannels, analytically. The physical properties of the fluid and walls were considered constant; the fluid was incompressible and mono component, as the result the mass diffusion phenomenon was ignored. They found that the minimum total entropy generation rate happened for an individual slip velocity.

Anand (2014) used power law fluid as the working fluid and studied the effects of three different slip laws such as non-linear Navier, Hatzikiriakos and asymptotic on heat transfer and entropy generation of pressure driven flow, analytically. For this purpose he considered a rectangular microchannel under uniform heat flux boundary condition. For a similar slip coefficient, the Nusselt number and average entropy generation rate predicted utilizing different slip laws were not the same. Also he showed that the effect of slip on entropy generation due to heat transfer is significant and has to be considered. Two-dimensional analysis is the shortcoming of this study.

Vinodhan and Rajan (2014) numerically studied several new microchannel heat sink designs. They utilized water as the working fluid and divided the heat sink into four quadrants, each of them having a separate entry and exit. After some minor modification with respect to the microchannel length, they used the I-type heat sink of Chein and Chen (2009) as the conventional heat sink. They showed the bottom plate temperature gradients in the new designs are lower than that in conventional heat sink, because of more uniform distribution of coolant into different microchannels. Also thermal resistance in the new microchannel heat sink designs compared with the conventional heat sink was lower. Utilization of independent properties is the deficiency of this study.

Duryodhan et al. (2015) studied heat transfer in diverging and converging three-dimensional microchannels experimentally; also they performed three dimensional numerical simulations. Their numerical results showed that heat flux distribution in diverging microchannels was different from that of the converging ones due to conjugate effects. Their results showed that diverging and converging microchannels exhibit better thermo-hydraulic performance compared with constant cross-section microchannels. Therefore, for a single phase liquid heating they are better choices.

Dehghan et al. (2015) studied heat transfer enhancement in converging flow passage rectangular

MCHS utilizing water. Their results showed that with increased tapering the Poiseuille number augmented, while the required pumping power decreased. Also, with tapering the Nusselt number and the convection heat transfer coefficient increased.

Based on the findings of the previous studies, heat transfer from the solid to fluid in a microchannel heat sink increases by: increasing heat transfer surface using fins (Vanapalli *et al.* (2007)), optimizing the design of the microchannel heat sink (Li and Peterson (2006)), optimizing the cross-section of microchannel (Nonino *et al.* (2010)) and using proper flow entry/exit configurations (Chein and Chen (2009)).

In most of the previous studies on MCHS, the computational domain consisted only of a single channel and a slice of wall, for which symmetrical boundary condition was used. Also previous studies on different entry/exit configurations effects on microchannel heat sink performance were limited to the rectangular microchannel heat sinks. For cooling electronic chips which are in an unwanted trapezoidal space a heat sink with trapezoidal geometry may be needed. In the present study, a trapezoidal MCHS, consisting of five trapezoidal microchannels, has been considered. The computational domain includes the geometric configuration and location of the entry and exit, the flow through microchannels and the solid parts of the heat sink. The effects of different entry/exit configurations, which have rarely been considered, are investigated. For this purpose the properties variations of water and silicon with temperature are considered and their effects on the MCHS performance are quantified.

2. GEOMETRIC CONFIGURATIONS

The geometry and general dimensions of the A-type heat sink and the isosceles trapezoidal microchannels are shown in Fig. 1. As noticed, the horizontal entry and exit are situated at the center of the north and the south walls. In practice, the heat generating electronic chip is attached to the substrate of the heat sink. As denoted in Fig. 2, for the ease of discussion the channels are numbered from the left to the right. All solid parts of the heat sink are made of silicon and the working fluid is considered to be water.

To examine the effects of entry/exit configuration on heat transfer and fluid flow, in addition to the previously specified configuration, three other configurations have been considered. As shown in Fig. 3, these configurations are called the B-, C- and D-type. Other than change of entry/exit locations, all of the geometric dimensions of other configurations are the same as those shown in Fig. 1 for the A-type configuration. In the B-type heat sink, the entry and exit have been moved from the centers of the north and south walls to the right edge of the entry plenum and the left edge of the exit plenum, respectively. In the C-type heat sink, the entry and exit are located on the west wall at the center of the entry and exit plenums. In the D-type heat sink, the entry is on the

east wall at the center of the entry plenum and the exit is on the west wall at the center of the exit plenum.
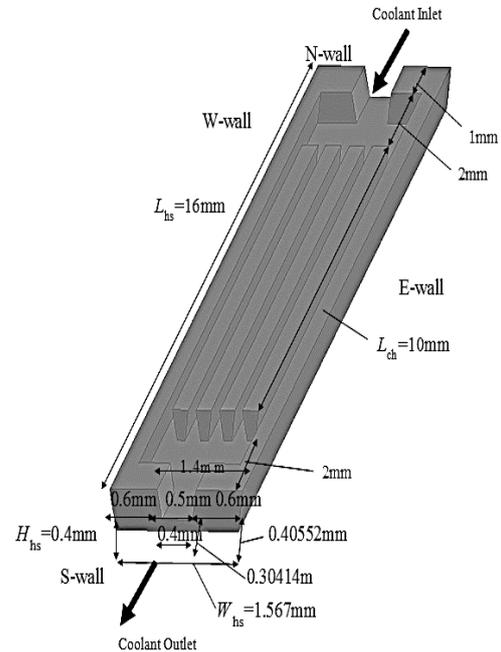

Fig. 1. Geometric configuration of the A-type microchannel heat sink.
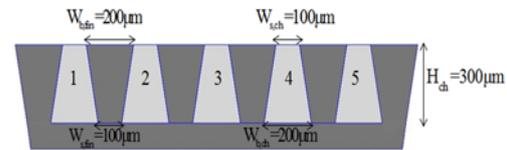

Fig. 2. Fin and microchannel dimensions.

3. THE GOVERNING EQUATIONS AND BOUNDARY CONDITIONS

To drive the governing equations, the following assumptions have been taken into account:

1. The three-dimensional laminar fluid flow and heat transfer are steady.

2. The properties of water and solid parts of the heat sink are temperature dependent.

3. The external surfaces of heat sink including the side walls and the top wall, which creates the flow passage in every microchannel, are all assumed to be insulated.

According to the above assumptions, the continuity, momentum and energy balance equations are:

Continuity:

$$\frac{\partial}{\partial x}(\rho u) + \frac{\partial}{\partial y}(\rho v) + \frac{\partial}{\partial z}(\rho w) = 0 \qquad (1)$$

Momentum:

$$\frac{\partial}{\partial x}(\rho uu) + \frac{\partial}{\partial y}(\rho vu) + \frac{\partial}{\partial z}(\rho wu)$$
$$= -\frac{\partial p}{\partial x} + \frac{\partial}{\partial x}\left(\mu\frac{\partial u}{\partial x}\right) +$$
$$\frac{\partial}{\partial y}\left(\mu\frac{\partial u}{\partial y}\right) + \frac{\partial}{\partial z}\left(\mu\frac{\partial u}{\partial z}\right) \tag{2}$$

$$\frac{\partial}{\partial x}(\rho uv) + \frac{\partial}{\partial y}(\rho vv) + \frac{\partial}{\partial z}(\rho wv)$$
$$= -\frac{\partial p}{\partial y} + \frac{\partial}{\partial x}\left(\mu\frac{\partial v}{\partial x}\right)$$
$$+ \frac{\partial}{\partial y}\left(\mu\frac{\partial v}{\partial y}\right) + \frac{\partial}{\partial z}\left(\mu\frac{\partial v}{\partial z}\right) \tag{3}$$

$$\frac{\partial}{\partial x}(\rho uw) + \frac{\partial}{\partial y}(\rho vw) + \frac{\partial}{\partial z}(\rho ww)$$
$$= -\frac{\partial p}{\partial z} + \frac{\partial}{\partial x}\left(\mu\frac{\partial w}{\partial x}\right)$$
$$+ \frac{\partial}{\partial y}\left(\mu\frac{\partial w}{\partial y}\right) + \frac{\partial}{\partial z}\left(\mu\frac{\partial w}{\partial z}\right) \tag{4}$$

Energy in the fluid part:

$$\frac{\partial}{\partial x}(\rho uT) + \frac{\partial}{\partial y}(\rho vT) + \frac{\partial}{\partial z}(\rho wT)$$
$$= \frac{\partial}{\partial x}\left(\frac{k}{c_p}\frac{\partial T}{\partial x}\right) + \frac{\partial}{\partial y}\left(\frac{k}{c_p}\frac{\partial T}{\partial y}\right)$$
$$+ \frac{\partial}{\partial z}\left(\frac{k}{c_p}\frac{\partial T}{\partial z}\right) \tag{5}$$

Energy in the solid parts is:

$$\frac{\partial}{\partial x}\left(k_s\frac{\partial T}{\partial x}\right) + \frac{\partial}{\partial y}\left(k_s\frac{\partial T}{\partial y}\right)$$
$$+ \frac{\partial}{\partial z}\left(k_s\frac{\partial T}{\partial z}\right) = 0 \tag{6}$$

The boundary conditions are related to the heat sink operational conditions. In practical applications, to receive heat and dissipate it by the fluid flow, heat sink is attached to an electronic chip, which generates heat. A pump delivers the fluid at a given temperature and mass flow rate. The pressure loss is dependent on the flow rate, thus flow rate or pressure loss can be taken as constants for the simulations. In this study, similar to the study of Li *et al.* (2004), the pressure drop is adopted. The pressure loss from entry to exit is defined as:

$$\Delta p = p_{in} - p_{out} \tag{7}$$
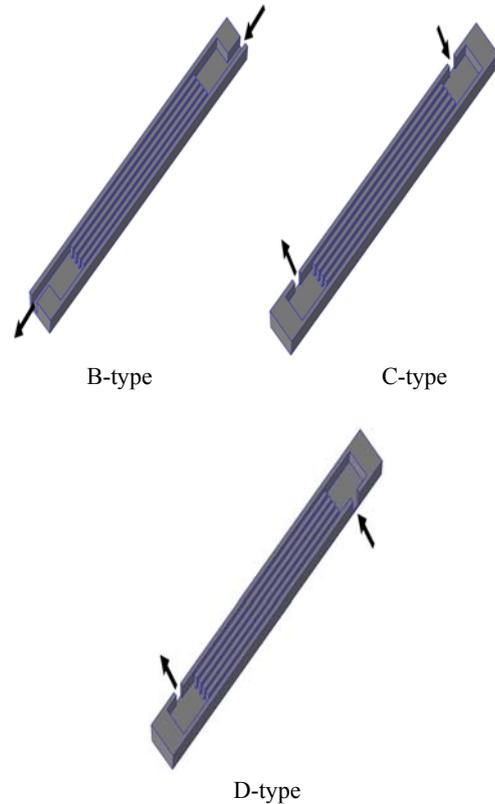
Entry:

$$p = p_{in}, \qquad T = T_{in} \tag{8}$$

Exit:

$$p = p_{out}, \qquad \frac{\partial T}{\partial n} = 0 \tag{9}$$

Fluid-solid interfaces:

$$\vec{V} = 0, \quad T_f = T_s, \quad -k_s\frac{\partial T_s}{\partial n} = -k_f\frac{\partial T_f}{\partial n} \tag{10}$$

At the substrate:

$$q_w = -k_s\frac{\partial T_s}{\partial n} \tag{11}$$

Fig. 3. The geometry showing the B-, C- and D-type entry/exit configurations.

T_{in} and p_{in} and are the fluid entry temperature and pressure, respectively. p_{out} is the exit pressure, n is the direction normal to the specified wall or the exit plane. The substrate is subjected to a heat flux of q_w=200kW/m².

As seen from Eq. (10), the non-slip condition has been assumed for every solid-liquid interface.

The thermo-physical properties of pure water taken from Bergman *et al.* (2011), within the temperature range of 300 to 325 K, have been curve fitted by MATLAB using the exponential method with correlation coefficient better than 95%. Also the temperature dependent thermal conductivity of silicon has been taken from Glassbrenner and Slack (1964). The results are:

$$k_f = 0.3424\exp(0.00195T) - 0.00163 \tag{12}$$

$$\mu_f = 57.83\exp(-0.04053T)$$
$$+ 0.01473\exp(-0.01095T) \tag{13}$$

$$\rho_f = 1130\exp(-0.0004173T) \tag{14}$$

$$c_{p,f} = 6.747\times10^8\exp(-0.05862T)$$
$$+ 3989\exp(0.0001428T) \tag{15}$$

$$k_{Silicon} = 290 - 0.4T \qquad (16)$$

4. PERFORMANCE EVALUATION INDEXES

To evaluate the overall performance of the heat sink several indexes are utilized normally. These indexes are explained in the following sub sections.

4.1 Average Nusselt Number

Based on the Newton's law of cooling, the total heat transfer in a heat sink is:

$$q_w = \overline{h}\left(T_{hs,avg} - T_{avg}\right) \qquad (17)$$

Where $T_{hs,avg}$ and T_{avg} are the heat sink and coolant average temperatures, respectively.

The average Nusselt number, as a thermal performance index, is defined as:

$$\overline{Nu} = \frac{\overline{h}D_h}{k_f} \qquad (18)$$

Where $\overline{h}$ is the heat transfer coefficient, which is calculated via Eq. (17), and D_h is the hydraulic diameter of every channel evaluated as:

$$D_h = \frac{4A}{p} \qquad (19)$$

4.2 Total Thermal Resistance

The total thermal resistance of any microchannel heat sink is the sum of conductive and convective resistances (Chai *et al.* (2013)). The conductive resistance is not dependent on pressure drop, whereas when the pressure drop increases (for instance the flow rate enhances) the convective resistance declines (Chai *et al.* (2013)). The total thermal resistance of the heat sink is:

$$R_{th} = \frac{T_{w,max} - T_{in}}{q_w W_{hs} L_{hs}} \qquad (20)$$

where $T_{w,max}$ is the heat sink base plate maximum temperature.

4.3 Non-uniformity of Base Plate Temperature

Decreasing the temperature of the base plate is an important objective of designing new configurations for microchannel heat sinks. Difference between the maximum and the minimum base plate temperatures is smaller when the cooling is more uniform. Theta is the ratio of difference between the maximum and minimum base plate temperatures to the heat flux, defined as:

$$\theta = \frac{T_{b,max} - T_{b,min}}{q_w} \qquad (21)$$

θ is regarded as the measure of non-uniformity of the base plate temperature.

5. NUMERICAL PROCEDURE

The three-dimensional governing equations with the associated boundary conditions for fluid flow and heat transfer have been solved using an element-based finite volume method utilizing the ANSYS CFX commercial code. Auto time scale factor is employed for the continuity, momentum and energy equations. Also high resolution scheme is used to discretize the equations. In the following two sub-sections the results of validation and mesh refinement studies are presented.

5.1 Validation

In order to make sure about the validity of the computational method and the numerical results, solutions were obtained for the three dimensional MCHS used in the numerical study of Chein and Chen (2009) also in the experimental study of Phillips (1988). As shown in Fig. 4, the MCHS utilized for the validation study consists of 11 rectangular microchannels. In the studies of Chein and Chen (2009) and Phillips (1988) the working fluid was water. For the validation study three pressures drops of 25, 35 and 50 kPa and the heat flux of 1000 kW/m^2 were assumed and a grid system with 891372 elements for the same geometry of Chein and Chen (2009) and Phillips (1988) was adopted. The average Nusselt number values obtained in this study have been compared with those of Chein and Chen (2009) in Fig. 5. Also in Fig. 6 the local Nusselt number values along the microchannel #5 have been compared with those of Philips (1988), for the pressure drop of 50 kPa and the heat flux of 1000 kW/m^2. The trend of local Nusselt number change along microchannel #5 is the same as that of Philips (1988). Also the maximum relative difference between the average Nusselt number obtained in this study and that of Chein and Chen (2009) is less 3%, which is for pressure drop of 50 kPa. Thus the validity of the computational method and the numerical results of this study are stated.
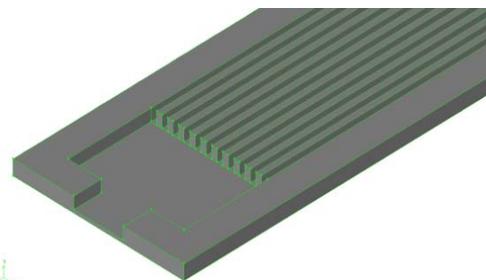

Fig. 4. The geometry of Chein and Chen (2009) and Philips (1988); utilized here for the validation study.

5.2. Grid Independency Test

To check the mesh independency of the results, solutions were obtained by utilizing three grid
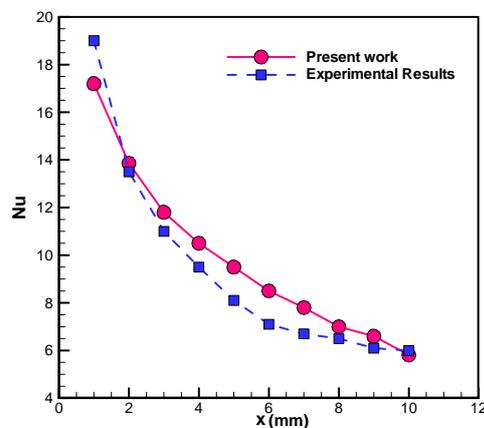
systems: 1) coarse with 391680 elements, 2) fine with 673920 elements and 3) very fine with 1365740 elements for the A-type heat sink, ∆P=15 kPa and q_w=200 kW/m². The streamlines in the mid-plane of the entry and exit plenums for the three mentioned grid systems were studied and they were generally the same. The average Nusselt numbers obtained have been reported in Table 1. The Nusselt number for the very fine grid is only 0.34% higher than that of the fine one; therefore the grid system with 673920 elements seems to be fine enough. In order to ensure grid independency of the results, temperature variation along bottom center of microchannel #3(fluid-solid interface) for the A- type MCHS, obtained using three different grids, has been shown in Fig. 7. As shown the fine grid system is appropriate, hence was used for all of further simulations for the A-type MCHS. It should be noted that from the sum of 673920 elements, 406080 elements are in the solid part and 267840 elements are in the fluid part.
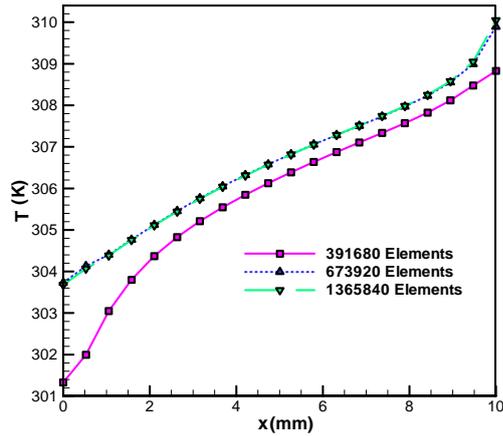
Fig. 7. Temperature along bottom center of microchannel #3 in A-type MCHS using three different grid systems; ∆P=15 kPa and q_w =200 kW/m².
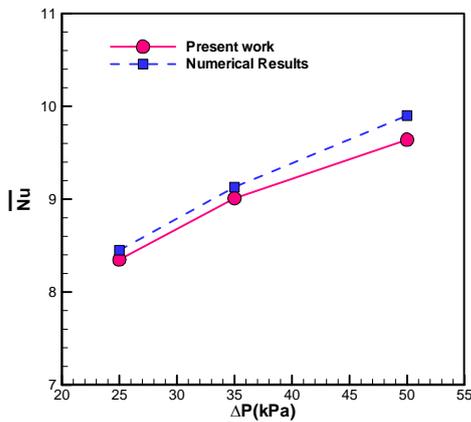
Fig. 5. The average Nusselt number obtained in the present study and that of Chein and Chen (2009) for three pressure drops of 25, 35 and 50 kPa.

Table 1 The average Nusselt number for water and A-type heat sink utilizing different grid systems; ∆P=15 kPa and q_w =200 kW/m²

	Number of elements	Average Nusselt number	Relative difference%
Coarse	391680	14.299	-
Fine	673920	14.846	3.82
Very fine	1365840	14.897	0.34

As assumed by Chein and Chuang (2007), if heat loss to the environment is neglected, the energy absorbed by the working fluid is:

$$Q_{flow} = \dot{m}\, c_p \left(T_{out} - T_{in} \right) \tag{22}$$

Percentage of relative difference =

$$\left| \frac{Q_{flow} - q_w W_{hs} L_{hs}}{q_w W_{hs} L_{hs}} \right| \times 100 \tag{23}$$

Where $\dot{m}$ is the mass flow rate and T_{in} and T_{out} are the fluid entry and exit temperatures, respectively. In theory, at steady state conditions the absorbed heat rate by the working fluid must be equal to the applied heat rate. However, the numerical results commonly show a small difference, which can be attributed to the utilized grid system. For instance, the maximum relative difference between the absorbed and applied heat rates in the study of Chein and Chen (2009) for straight entry/exit configuration was 5.4%. To find which heat sink geometry, in terms of entry/exit configuration, is more critical based on the difference between the applied and removed heat rates, solutions were obtained for all of the heat sink types. For this purpose water was used as the working fluid under ∆P=15 kPa and q_w=200 kW/m² and almost the same number of grids were utilized for all of the nominated types. In Table 2, the percentage of relative difference between the applied

Fig. 6. Variation of local Nusselt number along microchannel #5 in the present study and in the experimental study of Philips (1988) for ∆P=15 kPa.

heat rate to the heat sink and the heat absorbed have been presented for four types of heat sinks employed. The maximum relative difference between the absorbed and applied heat rates is 5.42%, which is for the A-type heat sink, indicating that the most crucial type is the A-type heat sink. It should be noted that the difference between the maximum and the minimum mesh numbers is only 44280, which is acceptable according to the range of the utilized number of meshes. This restates that the grid system having around 673920 elements, utilized for the A-type heat sink, is suitable for the other types; thus was adopted for all further simulations.

Table 2 Heat absorbed by water and the relative difference between the absorbed and applied heats for different heat sink types

Type	Elements	Q_{flow} (W)	Percentage of relative difference (%)
A	673920	4.741	5.42
B	629640	4.860	3.06
C	633960	4.985	0.56
D	633960	4.984	0.57

6. RESULTS AND DISCUSSION

The simulations have been performed for three pressure drops of 5, 10 and 15 kPa and the heat flux has been considered 200 kW/m². In the following subsections the results obtained for different performance characteristics of the trapezoidal microchannel heat sinks of this study are presented and discussed.

6.1 The Average Velocity Through Different Microchannels

The average fluid velocity in different microchannels at pressure drop of 5, 10 and 15 kPa for the four studied entry/exit configurations has been shown in Fig. 8. By reducing the pressure drop, the overall mass flow rate reduces, so the input flow rate into each microchannel decreases. However, as the pressure drop increases, the secondary flow in the entry and exit plenums amplifies and as a result the difference between the maximum and minimum velocity in different microchannels enhances.

As noticed from Fig. 8, for every specified configuration the average velocity in different microchannels is not the same. Also the maximum average velocity for the A-, B-, C- and D-type configurations have occurred in the microchannels #3, #4, #5 and #1, respectively.

To explain the reason for the velocity differences in different microchannels, the details of the flow in the entry plenum for all of the configurations have been studied. For instance, for the four selected configurations the streamlines in the mid-plane of the entry plenum at pressure drop of 15 kPa, have

been shown in Fig. 9. As can be seen the flow pattern in the entry plenum for every entry configuration is distinct and the details of the creation of recirculation zones, in terms of location and size, are also different. For the A-type configuration, two strong recirculation zones are formed at the left and right sides of the entry stream to the entry plenum. These are the main cause of pressure drop as flow expands in the entry plenum. However, for the A-type configuration, the microchannel #3 is in the direction of the entering flow, but out of the recirculation zones at the left and right sides of the plenum. Thus, the pressure drop from the entry to the entry to microchannel #3 is smaller, when compared to that for other microchannels. As a result, the average velocity in the microchannel #3 is more than that of other microchannels. Also for the A-type configuration, due to symmetry of the recirculation zones formed in the entry plenum, the average velocity of fluid passing through the microchannels #1 and #2 is exactly the same as those of microchannels #5 and #4, respectively.

For the B-type configuration, for which the entrance is at the right hand side of the north wall, a strong recirculation has formed at the left side of the entry plenum. However, the microchannel #4 is alongside the heat sink entrance and the pressure drop in the plenum from the entry to the entrance of the microchannel #4 is the minimum; thus the maximum average velocity has occurred in microchannel #4. For the C and D-type configurations, for which the flow enters the entry plenum from the western and eastern walls, respectively, part of the entering flow collides with the opposite wall and three weak recirculation zones form at the upper side of the entry plenum; also a weak recirculation zone forms in the lower part of the plenum beneath the entry. Therefore, for the C and D-type entry/exit configurations the pressure drop in the entry plenum for the microchannels farther from the entrance is less; thus for them the maximum average velocity has occurred in the microchannels #5 and #1, respectively.

As indicated in Fig. 8, average velocity is in the range of 0.4 and 1.3 m/s, so the Reynolds number based on the microchannel hydraulic diameter is between 93 and 301. This verifies the validity of the assumption of laminar flow in the microchannels.

The hydrodynamic entrance length for laminar flow is calculated using the following approximation as (Bergman *et al.* 2011):

$$x_{fd,h} = 0.05 \, ReD_h \qquad (24)$$

The hydrodynamic entrance length of the microchannel #3 at pressure drop of 15 kPa for the A, B, C and D-type entry/exit configurations is 3, 2.9, 2.8 and 2.8 mm, respectively. It shows that the developing region is limited to less than 30% of the microchannel length; thus the flow regime along most of the microchannel length is fully developed.

6.2 The Flow Average Temperature in Different Microchannels

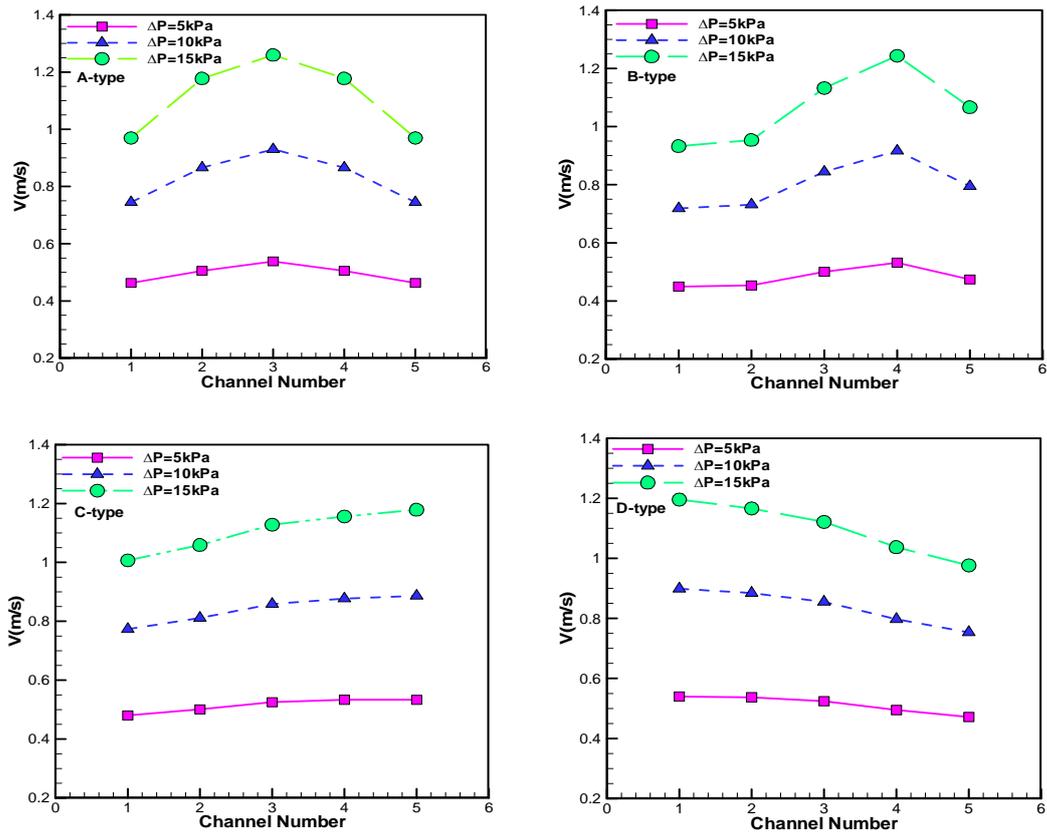Figure 10 shows the average flow temperature for the

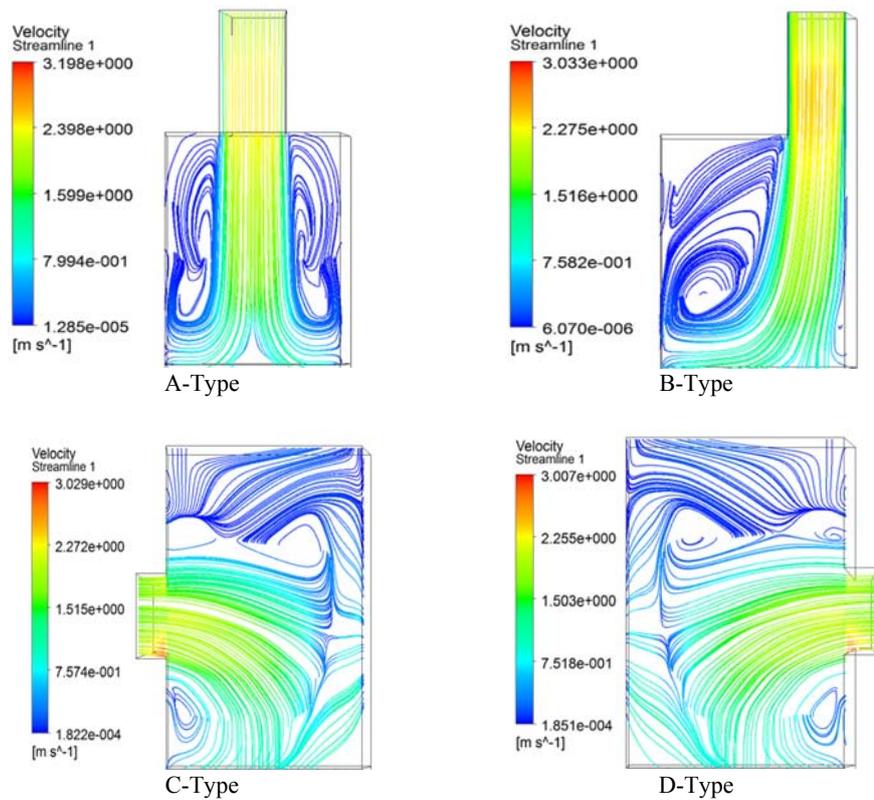**Fig. 8. Average velocity in different microchannels for different pressure drops.**

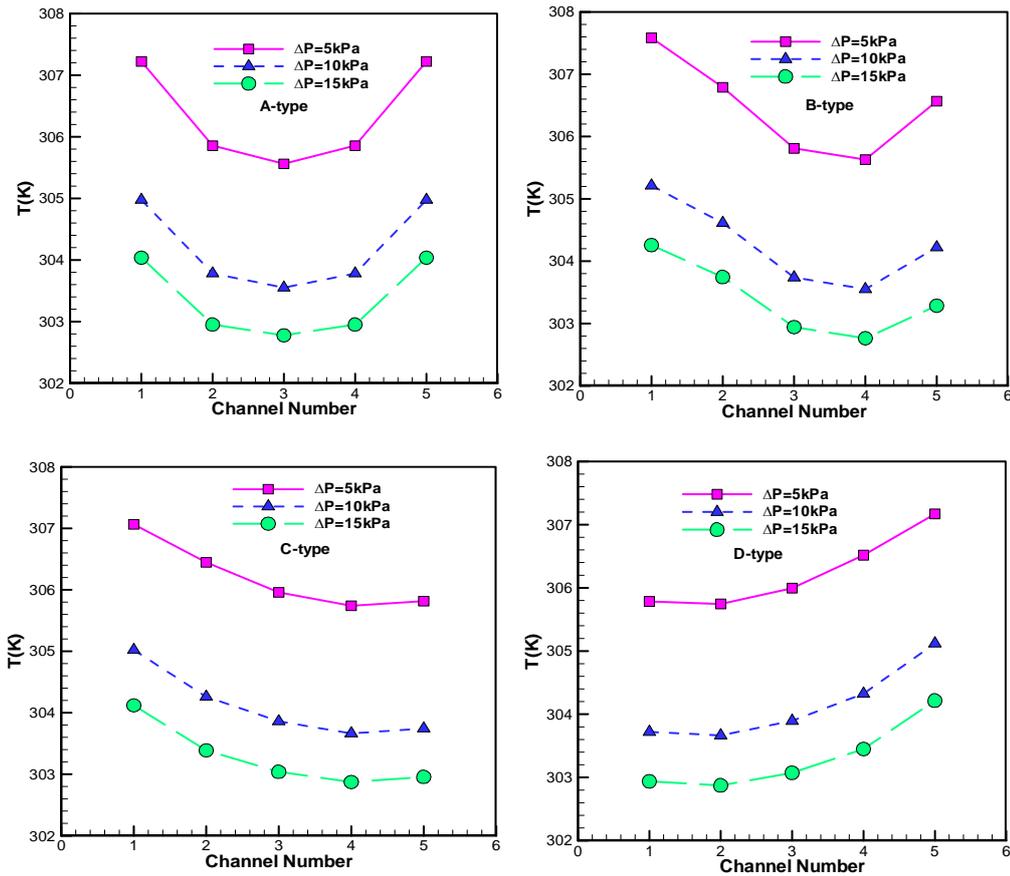**Fig. 9. Streamlines at mid plane of the** entry **plenum at ΔP=15 kPa.**

Fig. 10. The flow average temperature in different microchannels.

four selected entry/exit configurations and pressure drops of 5, 10 and 15 kPa. As shown in Fig. 10, with increasing pressure drop the average temperature in all of microchannels decreases for all of the nominated configurations. This is due to mass flow rate increase with pressure drop enhancement. It is noticed again that, for all of the configurations, the average flow temperature in the microchannels near the heat sink lateral walls is more than that of the adjacent one. For the A-type heat sink, the maximum and minimum temperatures occur in microchannels #1 (and #5) and #3, in which the minimum and maximum velocities occur, respectively. Also the maximum fluid temperature for the B, C and D-type heat sinks occur in the microchannels #1, #1 and #5, respectively. It should be noted that, due to more heat received from the side walls, the average flow temperature in the microchannels near the heat sink side walls is more than that of the adjacent one.

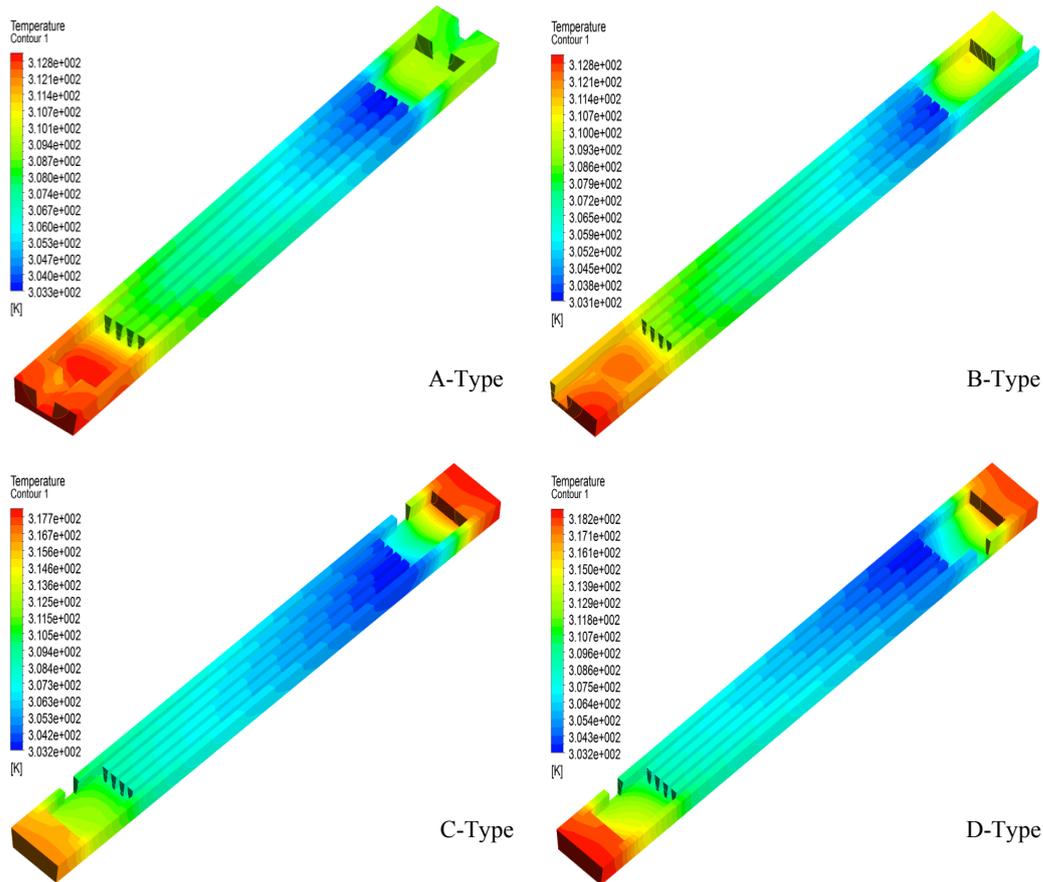## 6.3 Temperature Distribution in the MCHS Solid Part

As a sample, in Fig. 11 the temperature distribution across the solid parts of MCHS with various configurations is shown for pressure drop of 15 kPa. From Fig. 11, the non-uniformity of temperature distribution in the solid parts is evident, but the degree of this non-uniformity for different configurations is not the same. The highest temperature difference of the solid part has occurred

for the D-type heat sink and the lowest for the A-type, indicating that the A-type heat sink is better than the D-type as well as the other two types.

It is observed that, due to the absence of the heat removing microchannels at the head or end of MCHS, hot regions occur at its end. However, for the A and B-type heat sinks, for which the flow enters from the north wall and exits from the south wall, the head region of the solid part is generally at lower temperature compared with its end. Whereas, for the C and D types, for which the flow enters from one of the lateral walls, the solid head and end parts both are at higher temperatures compared with the rest. Also, for all of the entry/exit configurations, the low-temperature region has occurred at the beginning of the microchannels, where the fluid is at its lowest temperature and the heat transfer coefficient is greater.

6.4 Temperature Distribution on the Substrate of MCHS

By taking the advantage of the results of the numerical simulation, temperature distribution on the heat sink substrate for different conditions in terms of entry/exit configuration and pressure drop may be studied easily. Whereas, in every experimental study, it is usually difficult to measure temperature distribution on the substrate since it is attached either to the chip surface or the heat

Fig. 11. Temperature distribution in the solid part of MCHS with different entry/exit configurations at ΔP=15 kPa.
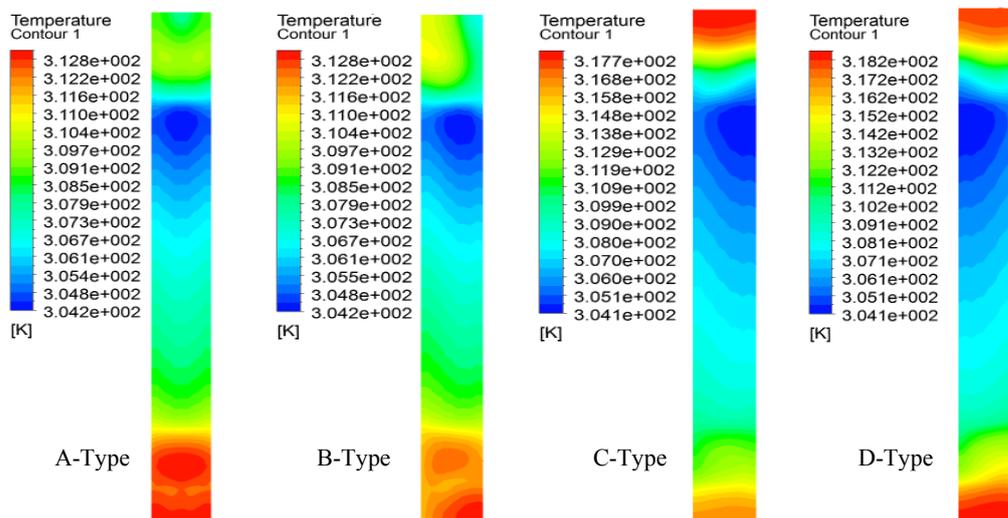
Fig. 12. Temperature distribution of the base plate of MCHS with different entry/exit configurations at ΔP=15 kPa.

generator. As an instance, the temperature distribution on the substrate of MCHS is presented in Fig. 12 for the four nominated types of entry/exit configurations at ΔP=15 kPa. As noticed, the detail

of temperature distribution depends on the entry/exit configuration, such that for the A and B- types, for which the entry is direct from the north wall, the region near the north wall is generally at lower

Table 3 Average Nusselt number for temperature-dependent and independent properties at ΔP=15 kPa

Average Nusselt number	A	B	C	D
Temperature-dependent properties of water and silicon	14.85	14.76	10.17	9.92
Temperature-independent properties of water, but variable conductivity of silicon	14.41	14.36	9.90	9.60
Relative difference for variable properties of water (%)	3.05	2.78	2.73	3.33
Temperature-independent properties of silicon, but variable properties of water	14.74	14.62	9.92	9.67
Relative difference for variable conductivity of silicon (%)	0.75	0.96	2.52	2.58

Table 4 Thermal resistance for temperature-dependent and independent properties at ΔP=15 kPa

Thermal resistance	A	B	C	D
Temperature-dependent properties of water and silicon	2.58	2.58	3.63	3.74
Temperature-independent properties of water, but variable conductivity of silicon	2.71	2.71	3.76	3.96
Relative difference for variable properties of water (%)	4.80	4.80	3.46	5.55
Temperature-independent properties of silicon, but variable properties of water	2.61	2.62	3.82	3.85
Relative difference for variable conductivity of silicon (%)	1.15	1.15	4.97	2.86

Table 5 Theta for temperature-dependent and independent properties at ΔP=15 kPa

Theta	A	B	C	D
Temperature-dependent properties of water and silicon	4.46e-5	4.45e-5	7.06e-5	7.33e-5
Temperature-independent properties of water, but variable conductivity of silicon	4.71e-5	4.70e-5	7.31e-5	8.25e-5
Relative difference for variable properties of water (%)	5.31	5.31	3.42	11.15
Temperature-independent properties of silicon, but variable properties of water	4.57e-5	4.57e-5	7.55e-5	7.63e-5
Relative difference for variable conductivity of silicon (%)	2.41	2.63	6.49	3.93

temperature compared to that for the C and D-types. Moreover, for the A and B-types the base plate enjoys from a more uniform distribution of temperature compared to the C and D-types. Also for all of the entry/exit configurations due to lack of convection, the top and bottom corners of the base plate are at relatively higher temperatures. Moreover, on the base plate a low temperature region occurs at the entrance region to the microchannels, because the coolant temperature is lower also heat removal coefficient is higher.

6.5 Effect of Temperature-Dependent Properties of the Coolant and Solid Parts on Performance Indexes of MCHS

To study the effects of variation of properties on overall thermal performance of the MCHS solutions were obtained for all of the nominated cases, for which both temperature-dependent properties as well as temperature-independent properties at 300 K were utilized. In Tables 3, 4 and 5 the values of average Nusselt number, thermal resistance and non-

uniformity of the base plate temperature have been presented for the four selected configurations, but only for pressure drop of 15 kPa. The results show that using the temperature-dependent properties instead of temperature-independent properties has desirable effect on thermal performance of the heat sink. As seen from Table 3, the use of temperature-dependent properties for water has increased the heat transfer between 2.73% and 3.33% and the maximum influence is for the D type configuration. Using temperature-dependent properties for silicon (solid parts) has increased the heat transfer between 0.75% and 2.58% and the maximum influence is again for the D type configuration. As seen from Table 4, the use of temperature-dependent properties for water has decreased the thermal resistance between 3.46% and 5.55% and the maximum effect is for the D type configuration. Using temperature-dependent properties for silicon has decreased the thermal resistance between 1.15% and 4.97% and the maximum influence is for the C type configuration. As seen from Table 5 the use of temperature-

dependent properties for water has decreased the maximum temperature difference on substrate surface divided by heat flux (theta) between 3.42% and 11.15% and the maximum effect is for the D type configuration. The use of temperature-dependent properties for silicon has decreased theta between 2.41% and 6.49% and the maximum influence is for the C type configuration.

6.6 Effect of Entry/Exit Configurations on Overall Thermal Performance of MCHS

To evaluate the overall performance of the heat sink, the results obtained for average Nusselt number, thermal resistance and the ratio of difference between the maximum and minimum base plate temperatures to the heat flux (θ) for different entry/exit configurations are discussed in this section.

Figure13 shows the average Nusselt number in terms of pressure drop for various entry/exit MCHS configurations. With enhancement of the pressure drop the mass flow rate of the fluid increases and the average fluid temperature decreases; hence, as indicated in Fig. 13, the average Nusselt number increases. Also as seen from Fig. 13, in terms of average Nusselt number the A-type heat sink is the best among the nominated types.
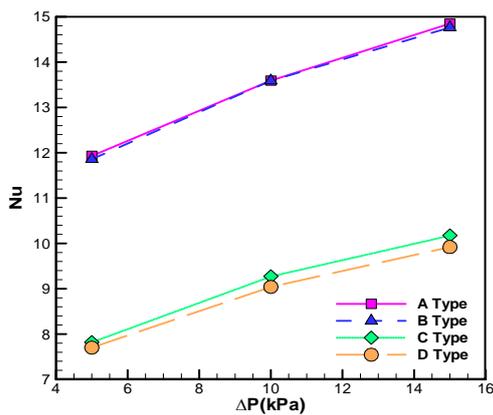

Fig. 13. Variation of average Nusselt number with pressure drop for various entry/exit configurations.

As seen from Fig. 14, which shows the change of thermal resistance with pressure drop, with increasing pressure drop the thermal resistance decreases for all of the heat sink types. With increasing pressure drop, the average velocity of the fluid rises and, as seen in Fig. 14, the heat transfer coefficient as well as the average Nusselt number enhance; thus both of the average fluid temperature and the average solid temperature decrease and according to Eq. (20), the thermal resistance decreases either. Also as seen from Fig. 14, in terms of thermal resistance again the A-type heat sink is the best among the nominated types.

The variation of θ has been shown in Fig. 15 for different heat sink types. As seen from Fig. 15, with increasing pressure drop θ decreases. As pressure drop increases, the mas flow rate and its velocity

enhance, which in turn the rate of heat transfer increases. As a result in overall the base plat temperature decreases and its distribution become more uniform. Also it is seen from Fig. 15 that for every pressure drop the A-type heat sink has the smallest θ; which indicates its better uniformity of the base plate temperature among all of the nominated entry/exit configurations.
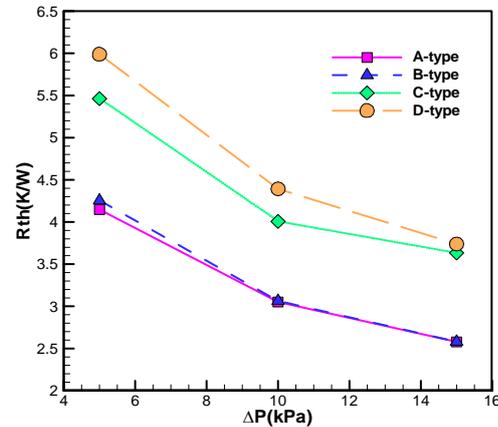

Fig. 14. Variation of thermal resistance with pressure drop for various entry/exit configurations.
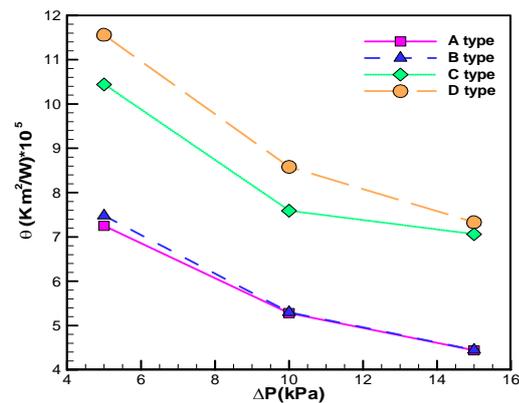

Fig. 15. Variation of theta with pressure drop for various entry/exit configurations.

7. CONCLUSION

Simulations have been performed for convective heat transfer of water in a trapezoidal MCHS with five trapezoidal microchannels and conduction through its solid parts. Effect of entry/exit configurations, pressure drop and temperature-dependent properties on thermal resistance, the average Nusselt number and temperature distribution in the microchannels as well as in the solid part of MCHS have been studied.

The following are a brief review of the conclusions:

1. Maximum average Nusselt number, minimum thermal resistance and minimum non-uniformity of the base plate temperature occur for the A-type, in which the coolant entry and exit are placed

horizontally at the center of the north and the south walls.

2. The A-type heat sink provides a more uniform temperature distribution in the solid part compared to other configurations.

3. The base plate temperature for the A and B-types is lower than those of the C and D-types, for which the entry and the exit are placed on the lateral walls.

4. Utilizing the temperature-dependent properties of water and silicon (solid parts) instead of temperature-independent properties showed desirable effect on thermal performance characteristics of the heat sink; such that the average Nusselt number enhanced and both of the thermal resistance and theta declined.

ACKNOWLEDGEMENTS

REFRENCES

Anand, V. (2014). Slip law effects on heat transfer and entropy generation of pressure driven flow of a power law fluid in a microchannel under uniform heat flux boundary condition. *Energy* 76, 716-732.

Bergman, T. L., F. P. Incropera and A. S. Lavine (2011). *Fundamentals of heat and mass transfer*, John Wiley and Sons.

Chai, L., G. Xia, M. Zhou, J. Li and J. Qi (2013). Optimum thermal design of interrupted microchannel heat sink with rectangular ribs in the transverse microchambers. *Applied Thermal Engineering* 51(1), 880-889.

Chein, R. and J. Chen (2009). Numerical study of the inlet/outlet arrangement effect on microchannel heat sink performance. International Journal of Thermal Sciences 48(8), 1627-1638.

Chein, R. and J. Chuang (2007). Experimental microchannel heat sink performance studies using nanofluids. *International Journal of Thermal Sciences* 46(1), 57-66.

Dehghan, M., M. Daneshipour, M. S. Valipour, R. Rafee and S. Saedodin (2015). Enhancing heat transfer in microchannel heat sinks using converging flow passages. *Energy Conversion and Management* 92, 244-250.

Duryodhan, V., A. Singh, S. Singh and A. Agrawal (2015). Convective heat transfer in diverging and converging microchannels. *International Journal of Heat and Mass Transfer* 80, 424-438.

Glassbrenner, C. and G. A. Slack (1964). Thermal conductivity of silicon and germanium from 3 K to the melting point. *Physical Review* 134(4A), A1058.

Guo, J., M. Xu, J. Cai and X. Huai (2011). Viscous dissipation effect on entropy generation in curved square microchannels. *Energy* 36(8), 5416-5423.

Guo, J., M. Xu, Y. Tao and X. Huai (2012). The effect of temperature-dependent viscosity on entropy generation in curved square microchannel. *Chemical Engineering and Processing: Process Intensification* 52, 85-91.

Hung, T. C. and W. M. Yan (2012). Effects of tapered-channel design on thermal performance of microchannel heat sink. *International Communications in Heat and Mass Transfer* 39(9), 1342-1347.

Ibáñez, G. and S. Cuevas (2010). Entropy generation minimization of a MHD (magnetohydrodynamic) flow in a microchannel. *Energy* 35(10), 4149-4155.

Ibáñez, G., A. López, J. Pantoja, J. Moreira and J. A. Reyes (2013). Optimum slip flow based on the minimization of entropy generation in parallel plate microchannels. *Energy* 50, 143-149.

Li, J. and G. Peterson (2006). Geometric optimization of a micro heat sink with liquid flow. *Components and Packaging Technologies, IEEE Transactions on* 29(1), 145-154.

Li, J., G. Peterson and P. Cheng (2004). Three-dimensional analysis of heat transfer in a micro-heat sink with single phase flow. *International Journal of Heat and Mass Transfer* 47(19), 4215-4231.

Nonino, C., S. Del Giudice and S. Savino (2010). Temperature-dependent viscosity and viscous dissipation effects in microchannel flows with uniform wall heat flux. *Heat Transfer Engineering* 31(8), 682-691.

Phillips, R. J. (1988). Microchannel Reat Sinks." *Lincoln Laboratory Journal* 1(1), 31-48.

Tuckerman, D. B. and R. Pease (1981). "High-performance heat sinking for VLSI." *Electron Device Letters, IEEE* 2(5): 126-129.

Vanapalli, S., H. Ter Brake, H. Jansen, J. Burger, H. Holland, T. Veenstra and M. Elwenspoek (2007). Pressure drop of laminar gas flows in a microchannel containing various pillar matrices. *Journal of Micromechanics and Microengineering* 17(7), 1381.

Vinodhan, V. L. and K. Rajan (2014). Computational analysis of new microchannel heat sink configurations. *Energy Conversion and Management* 86, 595-604.